Dalton Transactions

Cite this: *Dalton Trans.*, 2012, **41**, 4806

www.rsc.org/dalton

PAPER

Magnetic, electrochemical and spectroscopic properties of iron(III) amine–bis(phenolate) halide complexes†

Rebecca K. Dean,[a] Candace I. Fowler,[a] Kamrul Hasan,[a] Kagan Kerman,[b] Philip Kwong,[a] Simon Trudel,[c] Daniel B. Leznoff,[d] Heinz-Bernard Kraatz,[b] Louise N. Dawe[e] and Christopher M. Kozak‡*[a]

Received 22nd November 2011, Accepted 30th January 2012
DOI: 10.1039/c2dt12242a

Eight new iron(III) amine–bis(phenolate) complexes are reported. The reaction of anhydrous FeX_3 salts (where X = Cl or Br) with the diprotonated tripodal tetradentate ligands 2-tetrahydrofurfurylamino-*N*,*N*-bis(2-methylene-4,6-di-*tert*-butylphenol), H_2**L1**, 2-tetrahydrofurfurylamino-*N*,*N*-bis(2-methylene-4-methyl-6-*tert*-butylphenol), H_2**L2**, and 2-methoxyethylamino-*N*,*N*-bis(2-methylene-4,6-di-*tert*-butylphenol), H_2**L3**, 2-methoxyethylamino-*N*,*N*-bis(2-methylene-4-methyl-6-*tert*-butylphenol), H_2**L4** produces the trigonal bipyramidal iron(III) complexes, **L1**FeCl (**1a**), **L1**FeBr (**1b**), **L2**FeCl (**2a**), **L2**FeBr (**2b**), **L3**FeCl (**3a**), **L3**FeBr (**3b**), **L4**FeCl (**4a**), and **L4**FeBr (**4b**). All complexes have been characterized using electronic absorption spectroscopy, cyclic voltammetry and room temperature magnetic measurements. Variable temperature magnetic data were acquired for complexes **2b**, **3a** and **4b**. Variable temperature Mössbauer spectra were obtained for **2b**, **3a** and **4b**. Single crystal X-ray molecular structures have been determined for proligand H_2**L4** and complexes **1b**, **2b**, and **4b**.

Introduction

The amine–bis(phenolate) family of ligands has been used extensively with early transition metals, in particular groups 4 and 5,[1–27] and group 3/lanthanides.[28–33] These ligands are very well suited to stabilizing electron-deficient, high oxidation-state metal centers due to the strong π-donor ability of the phenolate groups. In particular, these systems have been shown to be excellent for the stabilization of high-valent organometallic systems, such as Ti(IV),[10–20] Zr(IV)[3,11–13,21–25] and Ta(V)-complexes,[5,17,26,27] which have primarily been used as polymerization catalysts. These extremely versatile and modifiable ligands are also being used with the mid-to-late transition metals.[34–42] Complexes possessing diamine–bis(phenolate) ligands on Fe(III) have been reported and used as models for catechol dioxygenase enzymes and other non-heme iron centers.[43–45] Indeed, the magnetic and redox behavior of these complexes makes them suitable structural and functional models for a variety of non-heme iron proteins.

We and others have reported the synthesis, structure and spectroscopic behavior of a related class of Fe(III) complexes supported by diamine–bis(phenolate) ligands, and a multitude of salen–Fe(III)[46–51] and salan–Fe(III) complexes[39,44,52–59] (H_2salen = *N*,*N*′-bis(salicylidene)ethylenediamine; H_2salan = *N*,*N*′-bis(2-hydroxybenzyl)ethylenediamine) have been described. Contrary to the numerous reports of salen and salan ligands being used with Fe(III), there are much fewer examples of iron complexes bearing the related tripodal (atrane-like) diamine–bis(phenolate) ligands.[44,57,60,61] These ligands contain an *N*,*N*-dimethylethylenediamine rather than an *N*,*N*′-dimethylethylenediamine central fragment present in a salan ligand. Unlike the typical planar arrangement of donor atoms in salen or salan ligands, which leads to square pyramidal geometries, these ligands give trigonal bipyramidal structures around five-coordinate LFeX complexes (where X is a monodentate ligand, typically a halide). Ligand derivatives containing a pyridyl arm have also been paired with Fe(III) centers.[42,45,57,61–64] Other neutral donor pendant arms include ethers such as tetrahydrofurfuryl[41,61,65] or methoxy ethylene groups.[61] Alternatively, a third anionic donor such as a carboxylate group has been used,[62,66] as well as a related amine–tris(phenolate).[67,68] Lastly, tridentate ligand derivatives have also been applied to Fe(III) centers, where the pendant arm of the ligand contains a hydrocarbon fragment.[40,62,69] Monomeric Fe(III) complexes having trigonal bipyramidal geometries are still quite rare, however, these tripodal

[a]*Department of Chemistry, Memorial University of Newfoundland St. John's, Newfoundland A1B 3X7, Canada. E-mail: ckozak@mun.ca*
[b]*Department of Physical and Environmental Sciences, University of Toronto at Scarborough Toronto, Ontario M1C 1A4, Canada*
[c]*Department of Chemistry, University of Calgary, Calgary, Alberta T2N 1N4, Canada*
[d]*Department of Chemistry, Simon Fraser University Burnaby, British Columbia V5A 1S6, Canada*
[e]*X-ray Diffraction Laboratory, Centre for Chemical Analysis, Research and Training, Memorial University of Newfoundland, St. John's, Newfoundland A1B 3X7, Canada*

†Electronic supplementary information (ESI) available. CCDC reference numbers 847891 (H_2**L4**), 847892 (**1b**), 847893 (**2b**), 847894 (**4b**) contain the supplementary crystallographic data for this paper. For ESI and crystallographic data in CIF or other electronic format. See DOI: 10.1039/c2dt12242a

‡S. T. was at Simon Fraser University when this work was carried out. K. K. and H.-B. K. were at The University of Western Ontario when this work was carried out.

amine–bis(phenolate) ligands are strong σ- and π-donors that provide sufficient electron density at the Fe(III) center to stabilize a five-coordinate geometry. The *o*- and *p*-positions of the phenolates in the ligand influence the donor strength. Using alkyl groups (*t*-butyl or methyl) in the *o*- and *p*-positions provides both steric protection at the metal center (particularly *ortho* *t*-butyl groups) and also increases the electron-donating ability of the phenolates. Electron withdrawing substituents, such as *o*- and *p*-dihalides or *p*-nitro groups, decreases the electron donating ability of the phenolates and hence the Fe(III) centers in these complexes are more Lewis acidic. In turn, this leads to six-coordinate structures, usually by the incorporation of a solvent ligand or a catechol substrate.[42,44,54,60–61,70]

Fujii *et al.* have performed electronic and electrochemical studies of Fe(III) salen complexes and the proposed oxidation of these complexes yields Fe(III) phenoxyl radical species.[47] Salan ligands have also been shown to be non-innocent in electrochemical redox processes. Wieghardt *et al.* have shown metal phenolate complexes can exhibit redox behavior at either the metal or the ligand, depending on the metal used or the substituents on the phenolate group.[41,71] Indeed, our own prior work has demonstrated that tripodal amine–bis(phenolate) complexes of Cr[72] and Co[34] also exhibit oxidation at the ligand resulting in a phenolate–phenoxyl radical redox couple. Whereas the localization of the oxidation has been primarily put in context of modeling oxidative transformations catalyzed by iron-containing metalloenzymes, specifically galactose oxidase and cytochrome P450, the non-innocence of amine–bis(phenolates) can also be influential for other catalytic processes where single-electron-transfer mechanisms may be involved.

We are interested in the development of new iron-based catalysts for organic synthesis. As a result, we have explored the catalytic potential of iron complexes supported by various amine–bis(phenolate)s either as tridentate donors[69] or as tetradentate ligands bearing an additional pendant arm, such as a pyridyl or amino group.[57] For example, we reported iron(III) compounds bearing amine–bis(phenolate)–ether ligands effectively catalyze the cross-coupling of aromatic Grignard reagents with alkyl halides possessing β-hydrogens.[65] Herein we report the synthesis and the structural, spectroscopic, magnetic, and electrochemical properties of iron halide complexes of tetradentate amine–bis(phenolate)–ether ligands.

Results and discussion

Synthesis of ligands and metal complexes

The amine–bis(phenol)–ether proligands, H_2**L1** to H_2**L4** (Fig. 1) were prepared by modified literature procedures[13,23] employing Mannich condensation of 2,4-di-*tert*-butylphenol or 2-*tert*-butyl-4-methylphenol, formaldehyde and the corresponding primary amine in water.[65,73,74] The synthesis and full characterization of 2-methoxyethylamino-*N*,*N*-bis(2-methylene-4-methyl-6-*tert*-butylphenol), H_2**L4** are reported here. The difference in polarity between a tetrahydrofurfuryl and methoxyethyl group (the dipole moments of THF and diethyl ether, for example, are 1.7 and 1.2 D, respectively) and the rigidity of the tetrahydrofurfuryl group relative to the methoxy group should allow the study of the subtle effect of donor strength on the resulting electronic behavior of the metal complex. Single crystals of H_2**L4** suitable for X-ray diffraction were obtained from a saturated methanol solution. The structure of H_2**L4** is shown in Fig. 2, crystallographic data are given in Table 1, and selected bond lengths and angles are given in Table 2. ^{1}H and ^{13}C NMR analysis of H_2**L4** is consistent with the solid-state structure but show that in solution the hydrogen bonding interactions are easily broken allowing free rotation of the phenol fragments. The methylene protons located between the amine nitrogen and the phenol groups appear as singlets in $CDCl_3$ or acetone-d_6, whereas restricted rotation of the methylene group would lead to diastereotopic protons. The bond lengths and angles around each atom are consistent with those found in the structures of related ligands.

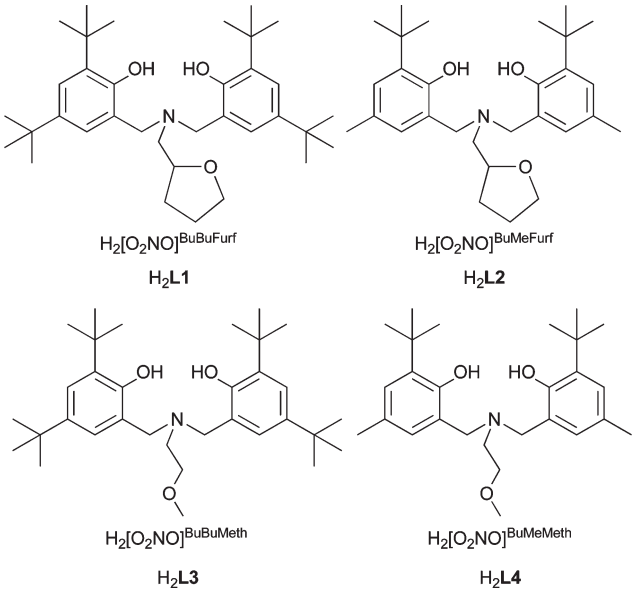

Fig. 1 Amine–bis(phenol)–ether proligands.

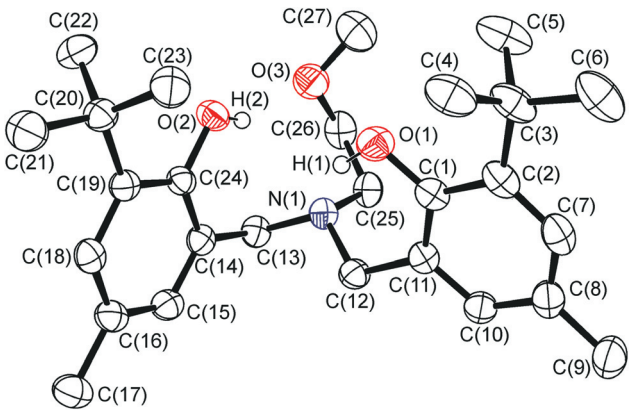

Fig. 2 Molecular structure (ORTEP) and numbering scheme of H_2**L4**. Ellipsoids are shown at 50% probability. Only –OH hydrogen atoms are shown.

The desired iron(III) complexes were obtained by dropwise addition of a methanol solution of FeX_3 (X = Cl, Br) to a methanolic slurry of the ligand at room temperature to yield a dark blue mixture. NEt_3 is added to neutralize the resulting solution (Scheme 1). The resulting complexes Fe**XL1** (**1a**, X = Cl; **1b**,

Table 1 Crystallographic and structure refinement data for H_2[$\mathbf{L_4}$], **1b**, **2b** and **4b**

Compound reference	H_2**L4**	**1b**	**2b**	**4b**
Chemical formula	$C_{27}H_{41}NO_3$	$C_{35}H_{53}BrFeNO_3$	$C_{29}H_{41}BrFeNO_3{\cdot}H_2O$	$C_{27}H_{39}BrFeNO_3$
Formula mass	427.63	671.56	605.40	561.35
Crystal system	Triclinic	Monoclinic	Monoclinic	Monoclinic
a/Å	10.1430(8)	14.923(13)	9.9384(7)	12.2762(19)
b/Å	11.1181(9)	11.6563(10)	24.9188(18)	11.1411(15)
c/Å	12.4742(11)	19.772(17)	12.5168(9)	19.870(3)
α (°)	98.858(7)	90.00	90.00	90.00
β (°)	110.988(8)	104.059(11)	95.852(2)	103.834(2)
γ (°)	100.462(7)	90.00	90.00	90.00
Unit cell volume/Å^3	1254.3(2)	3336(4)	3083.7(4)	2638.8(7)
T/K	138(2)	173(2)	113(2)	138(2)
Space group	$P\bar{1}$	$P2_1/c$	$P2_1/n$	$P2_1/c$
Z	2	4	4	4
Radiation type	Mo-Kα	Mo-Kα	Mo-Kα	Mo-Kα
Absorption coefficient, μ/mm^{-1}	0.072	1.684	1.816	2.113
No. of reflections measured	12 208	28 109	28 491	19 730
No. of independent reflections	5162	6865	7006	5406
R_{int}	0.0324	0.0805	0.0207	0.0282
Final R_1 values ($I > 2\sigma(I)$)[a]	0.0709	0.0775	0.0504	0.0502
Final w$R(F^2)$ values ($I > 2\sigma(I)$)[a]	0.1859	0.2126	0.1389	0.1295
Final R_1 values (all data)	0.0914	0.0862	0.0540	0.0545
Final w$R(F^2)$ values (all data)	0.2013	0.2220	0.1425	0.1326
Goodness of fit on F^2	1.033	1.093	1.054	1.101
CCDC reference	847891	847892	847893	847894

[a] $R_1 = \Sigma(|F_o|-|F_c|)/\Sigma|F_o|$); w$R_2 = [\Sigma(w(F_o^2-F_c^2)^2)/\Sigma w(F_o^2)^2]^{1/2}$.

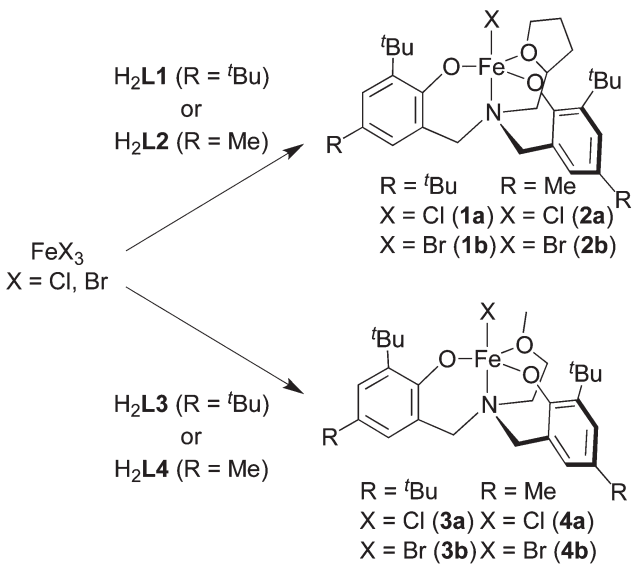

Scheme 1 Synthesis of iron(III) amine–bis(phenolate) complexes.

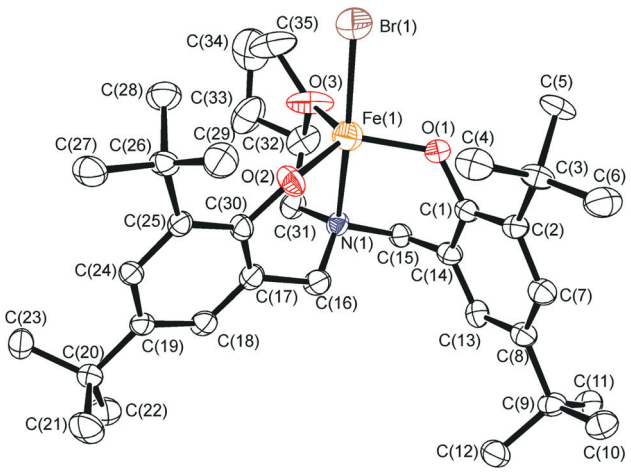

Fig. 3 Molecular structure (ORTEP) and numbering scheme of FeBr**L1** (**1b**). Ellipsoids are shown at 50% probability and H-atoms removed for clarity.

X = Br), FeX**L2** (**2a**, X = Cl; **2b**, X = Br), FeX**L3** (**3a**, X = Cl; **3b**, X = Br) and FeX**L4** (**4a**, X = Cl; **4b**, X = Br) are obtained as paramagnetic dark indigo powders that give analytically pure products upon recrystallization from methanol or acetone. The ^{1}H NMR spectra of these compounds show shifted and broadened resonances as a result of their paramagnetic nature, therefore MALDI-TOF mass spectrometry was useful in their characterization. In the presence of an anthracene matrix, the masses were observed corresponding to the parent and characteristic fragment ions, but in all complexes the parent ion corresponding to FeX**Ln** is relatively weak. The halide ion is only weakly coordinated to the metal and, therefore, the reference peak corresponds to the loss of halide, $[M - X]^+$, namely $[FeL1]^+$. The identity of the fragments was further confirmed by matching the isotopic patterns of the relevant peaks.

Single crystals suitable for X-ray diffraction were obtained for **1b**, **2b** and **4b**. Their structures are shown in Fig. 3–5, crystallographic data are given in Table 1, and selected bond lengths and angles are given in Table 3. We have previously reported the structure of the chloride-containing complex **2a**,[65,75] therefore the metric parameters of this compound are also given here for comparison. The coordination geometries around the iron atoms in all three structures are distorted trigonal bipyramidal and the

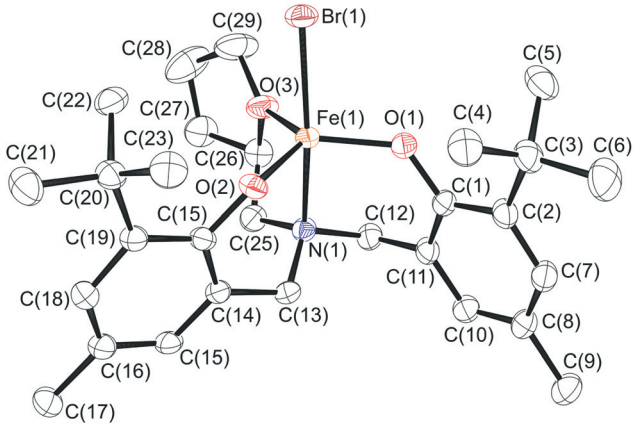

Fig. 4 Molecular structure (ORTEP) and numbering scheme of FeBr**L2** (**2b**). Ellipsoids are shown at 50% probability and H-atoms removed for clarity.

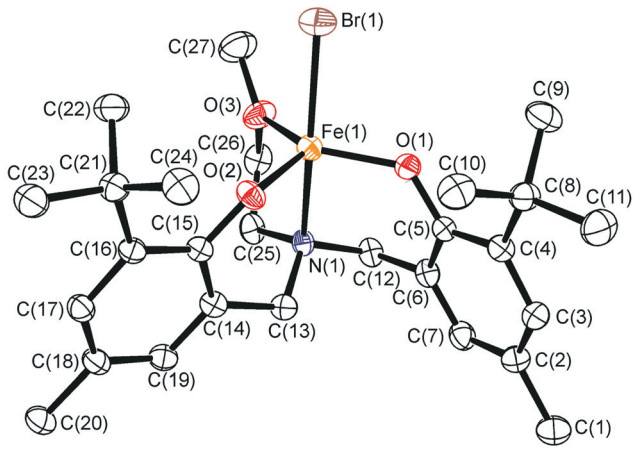

Fig. 5 Molecular structure (ORTEP) and numbering scheme of FeBr**L4** (**4b**). Ellipsoids are shown at 50% probability and H-atoms removed for clarity.

molecules are nearly isostructural. The metals are bonded to two phenolate oxygen atoms and the tetrahydrofurfuryl or methoxy oxygen atoms, which define the trigonal planes of the bipyramids. The central nitrogen atom of the ligands and the bromide ions occupy the apical sites. The Fe–O(1) and Fe–O(2) distances lie within the range of 1.834(4) to 1.866(2) Å for the phenolate oxygen donors and are similar to those observed in related trigonal bipyramidal iron(III) complexes possessing diamine bis(phenolate) ligands.[44,57] They are shorter, however, than the corresponding Fe–O bond lengths observed in 5-coordinate iron(III) chloride salen complexes, in which the Fe(III) ion adopts a square pyramidal geometry,[46,48,76] but similar in length to the Fe–O bonds in 5-coordinate iron(III) halide *salan* complexes.[39,57,59] However, they are shorter than the average Fe–O bond length of 1.92 Å observed in octahedral Fe(III) complexes.[42,44,45,61–63] The Fe–Br and Fe–N bond distances are in the ranges of 2.4034(16) to 2.4269(5) Å and 2.227(2) and 2.261(4) Å, respectively. The Fe–O(3) bond distance of 2.035(3) Å in **1b** is moderately shorter than those observed in the other

Table 2 Selected bond lengths (Å) and angles (°) for H_2**L4**

O(1)–C(1)	1.369(3)	O(1)–C(1)–C(2)	119.1(2)
O(2)–C(24)	1.370(3)	O(1)–C(1)–C(11)	119.9(2)
O(3)–C(26)	1.425(3)	C(27)–O(3)–C(26)	114.5(2)
O(3)–C(27)	1.410(4)	C(25)–N(1)–C(12)	111.85(18)
N(1)–C(25)	1.463(3)	C(25)–N(1)–C(13)	112.57(17)
N(1)–C(12)	1.477(3)	C(12)–N(1)–C(13)	109.80(17)
N(1)–C(13)	1.481(3)	O(3)–C(26)–C(25)	112.4(2)

tetrahydrofurfuryl-containing complexes, **2a** and **2b** (2.074(3) and 2.080(2) Å, respectively), which are in turn shorter than that observed in the acyclic ether-containing complex **4b**. The iron atoms are displaced by 0.211, 0.190 and 0.203 Å above the equatorial planes in **1b**, **2b** and **4b**, respectively. The N–Fe–Br angles lie in the range of 165.18(6) to 166.85° and are considerably distorted from the ideal linear geometry; they are bent away from the phenolate groups and directed toward the neutral-donor fragment. The Fe(1)–O(1)–C(*ipso*) and Fe(1)–O(2)–C(*ipso*) angles are similar in **2a**, **2b** and **4b** and exhibit a narrow range between 128.0(2) and 134.2(2)°. Also, whereas in complexes **1b**, **2a** and **2b** the bond angles in the equatorial plane around iron are each quite similar and close to 120°, the angles around the iron in **4b** are noticeably different from one another. The O(1)–Fe(1)–O(3) angle is 127.28(9)°, causing the other angles to pinch in. In summary, subtle structural deviations can occur as a result of seemingly minor modifications at both the 4-position of the phenolate ring and the pendant ether group. These structural effects manifest themselves in the spectroscopic and magnetic behavior of these complexes, which will be discussed below. The trigonality index, τ,[77] was calculated for each complex. Complex **1b** exhibits a value of 0.75, **2a** of 0.77, **2b** of 0.78, and **4b** of 0.63. For perfect trigonal bipyramidal and square pyramidal geometries the τ values are one and zero, respectively. The tetrahydrofurfuryl-containing complexes exhibit distorted trigonal bipyramidal geometries with τ values similar to those observed in other structurally characterized five-coordinate trigonal bipyramidal iron(III) complexes bearing tetradentate amine–bis(phenolate) ligands.[44,57] The methylether-containing complex, however, is much more distorted and approaches a structure intermediate to trigonal bipyramidal and square pyramidal.

Magnetic studies

All the iron(III) complexes have magnetic moments in solution in the range of 5.5–5.9 μ_B obtained by Evans' method at room temperature, consistent with high-spin d^5 ions. Variable temperature magnetic susceptibilities (χ_m) of **2b**, **3a** and **4b** were measured from 2 to 300 K and the plots of μ_{eff} *vs.* *T* for the three Fe(III) complexes are shown in Fig. 6. The magnetic moments at 300 K are 5.92, 5.50 and 5.67 μ_B for **2b**, **3a** and **4b**, respectively. The data for the three complexes show slow, smooth reductions in their moments as the temperature is lowered to 10 K. Below this temperature the moments drop more rapidly and at 2 K the observed magnetic moments are 3.91, 3.73 and 5.06 μ_B, respectively. The 300 K moments for these three complexes are as expected for a spin-only value for pure $S = 5/2$ spin states (μ_{eff} = 5.92 μ_B for 5 unpaired electrons). However, complex **2b** does

Table 3 Selected bond lengths (Å) and angles (°) for **1b**, **2a**, **2b** and **4b**

	1b	2a	2b	4b
Fe(1)–O(1)	1.840(3)	1.850(2)	1.8530(19)	1.866(2)
Fe(1)–O(2)	1.821(3)	1.854(2)	1.8531(19)	1.850(2)
Fe(1)–O(3)	2.035(3)	2.074(3)	2.080(2)	2.098(2)
Fe(1)–N(1)	2.261(4)	2.223(3)	2.227(2)	2.231(3)
Fe(1)–X(1)	2.4034(16)	2.2739(10)	2.4269(5)	2.4242(6)
O(1)–C(*ipso*)	1.335(5) "C1"	1.346(3) "C29"	1.347(3) "C1"	1.346(4) "C5"
O(2)–C(*ipso*)	1.338(5) "C30"	1.352(3) "C26"	1.356(3) "C24"	1.349(3) "C15"
O(1)–Fe(1)–O(2)	119.45(13)	118.39(10)	117.37(9)	113.45(10)
O(1)–Fe(1)–O(3)	121.34(12)	119.00(11)	120.14(9)	127.29(10)
O(2)–Fe(1)–O(3)	115.54(13)	119.60(11)	119.59(9)	115.97(10)
O(1)–Fe(1)–N(1)	86.91(13)	87.62(10)	89.18(8)	87.92(9)
O(2)–Fe(1)–N(1)	87.21(14)	89.37(10)	88.11(8)	88.69(9)
O(3)–Fe(1)–N(1)	76.72(13)	75.79(10)	75.99(8)	76.16(10)
O(1)–Fe(1)–X(1)	95.33(10)	96.60(8)	96.06(6)	94.53(7)
O(2)–Fe(1)–X(1)	103.29(12)	100.81(8)	100.07(6)	103.63(7)
O(3)–Fe(1)–X(1)	90.63(11)	89.98(8)	90.98(6)	90.85(7)
N(1)–Fe(1)–X(1)	166.27(8)	165.69(8)	166.85(6)	165.18(6)
Fe(1)–O(1)–C(*ipso*)	128.0(2)	129.3(2)	129.90(17)	131.00(19)
Fe(1)–O(2)–C(*ipso*)	134.2(2)	132.0(2)	131.93(17)	133.69(18)

Table 4 Mössbauer parameters for Fe**X**L**n**

Compound	*T*/K	δ^a/mm s^{-1}	ΔE_Q/mm s^{-1}
2b	297.6	0.39	1.22
	4.5	0.51	1.26
3a	295.0	0.29	0.72
	6.0	0.50	1.46
4b	295.0	0.38	0.90
	100.0	0.50	0.00
	30.0	0.50	1.22
	4.8	0.51	1.26

[a] With respect to Fe foil.

approach this value more so than **3a** and **4b**. There are no maxima observed in the plots of χ_m *vs.* *T* at any temperature and the magnetic data for all three compounds obey the Curie–Weiss law as shown by plots of χ^{-1} *vs.* *T*, from which Curie constants, *C*, and Weiss constants, θ, were obtained for **2b** ($C = 3.031$, $\theta = -3.26$ K), **3a** ($C = 3.785$ and $\theta = -1.88$ K) and **4b** ($C = 1.999$ and $\theta = -3.78$ K).

Mössbauer spectroscopy

Zero-field Mössbauer spectroscopy was used to investigate the spin behavior of three of these complexes and the relevant parameters are given in Table 4. The Mössbauer spectra of **2b** and **3a** were acquired first at room temperature (297.6 and 295.0 K, respectively) followed by low temperature (4.5 K and 6.0 K, respectively) and are shown in Fig. 7 and 8. The 297.6 K spectrum of **2b** was fit as an asymmetric doublet with both lines contributing an equal area. At low temperature the lines sharpen slightly and become more symmetric. At 297.6 K the isomer shift (δ) is 0.39 mm s^{-1} (*vs.* Fe foil) and quadrupole splitting with $\Delta E_Q = 1.22$ mm s^{-1}, whereas at 4.5 K $\delta = 0.51$ mm s^{-1} and $\Delta E_Q = 1.26$ mm s^{-1}. These values are consistent with a high spin Fe(III) ($S = 5/2$) center and similar to the parameters reported for a related Fe(III) diamine–bis(phenolate) (salan) complex.[59]

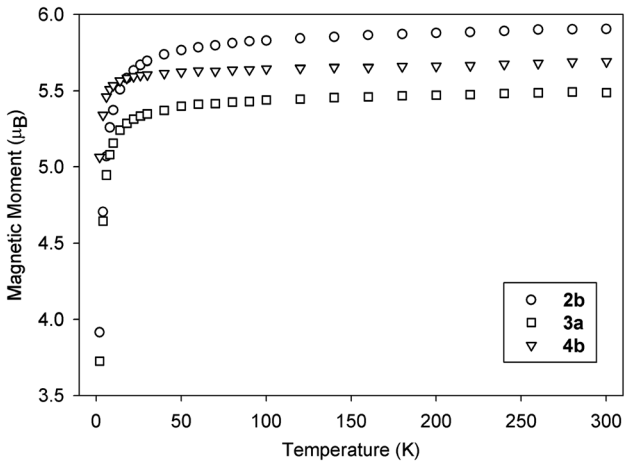

Fig. 6 Magnetic moment *vs.* temperature plots (◯ = **2b**, □ = **3a**, ▽ = **4b**).

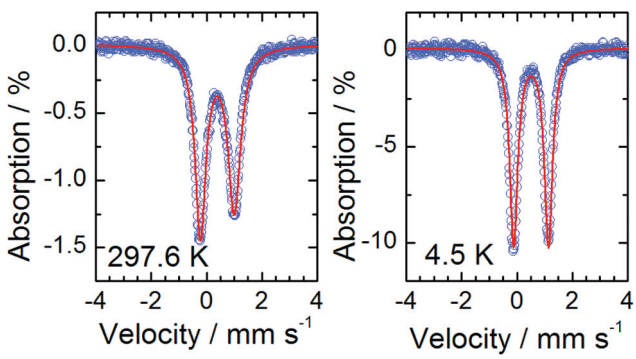

Fig. 7 Mössbauer spectra of **2b** recorded at 297.6 (left) and 4.5 K (right). The lines represent the best fit to the data (see text and Table 4).

The drop in moment may be attributed to zero-field splitting effects, saturation and intermolecular interactions. In any case, the 295 K data do give evidence that **2b** possesses a high spin ($S = 5/2$) configuration.

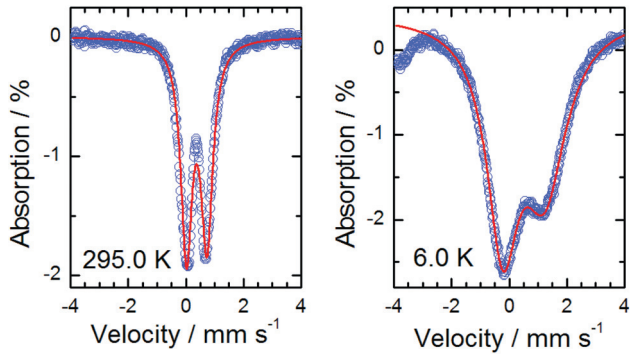

Fig. 8 Mössbauer spectra of **3a** recorded at 295.0 (left) and 6.0 K (right). The lines represent the best fit to the data (see text and Table 4).

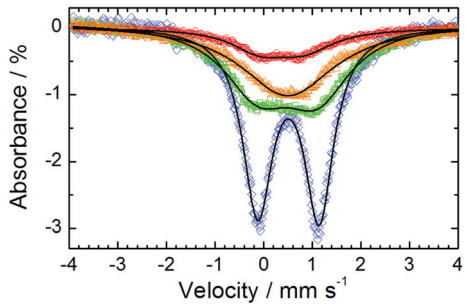

Fig. 9 Mössbauer spectra of **4b** recorded at (from top to bottom) 295.0 (red ◯), 100.0 (orange △), 30.0 (green □) and 4.8 K (blue ◇). The lines represent the best fit to the data (see text and Table 4).

The spectrum of **3a** (Fig. 8) at 295.0 K exhibits a slightly narrower doublet than for **2b**, with an isomer shift (δ) of 0.29 and ΔE_Q = 0.72 mm s^{-1}. At 6.0 K, the doublet broadens and shifts slightly to give δ = 0.50 mm s^{-1} and ΔE_Q = 1.46 mm s^{-1}. A similar broadening upon decreasing temperature at zero field has been observed in square pyramidal diamine–bis(phenolate) iron chloride complexes, and has been attributed to paramagnetic relaxation effects.[39]

The Mössbauer spectrum of **4b** is shown in Fig. 9. The spectrum is very broad at 295.0 K, but at 4.8 K it resolves into a doublet similar to that observed in the 4.5 K spectrum of **2b**. The isomer shifts and quadrupole splittings of **2b** and **4b** are identical at low temperature (for **4b** δ is 0.51 mm s^{-1} and ΔE_Q = 1.26 mm s^{-1}). The strong temperature-dependence of the Mössbauer spectrum for this complex is immediately apparent. The 100 K spectrum was fit using a single broad Lorentzian peak with an isomer shift (δ) of 0.50 mm s^{-1}. Below this temperature, the quadrupole splitting begins to increase so that the 30.0 K spectrum was fit using an asymmetric quadrupole-split doublet with δ = 0.50 mm s^{-1} and ΔE_Q = 1.22 mm s^{-1}. The 295.0 and 4.8 K isomer shifts and quadrupole splittings are consistent with high-spin Fe(III) states in asymmetric ligand environments. The Mössbauer parameters for all three compounds are nearly identical at near liquid helium temperatures.

Electronic spectroscopy

Electronic absorption spectra of the complexes show multiple intense bands in the UV and visible regions. In these complexes,

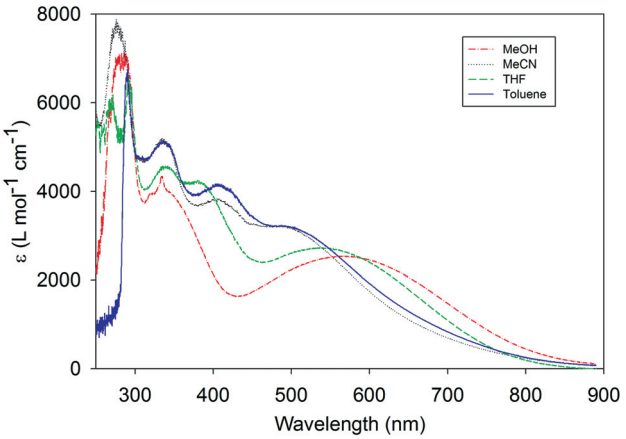

Fig. 10 Electronic absorption spectra of **1b** in methanol (red), acetonitrile (black), THF (green) and toluene (blue).

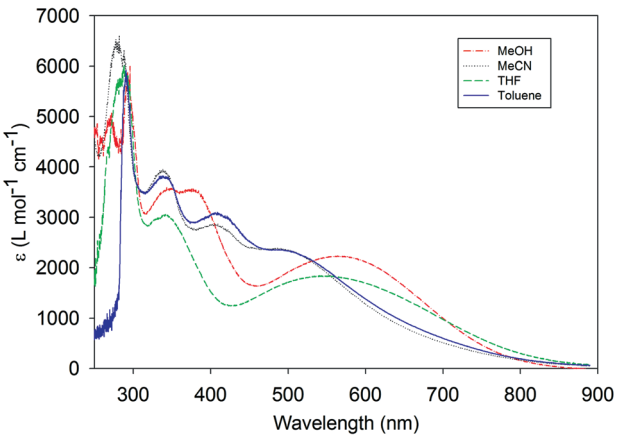

Fig. 11 Electronic absorption spectra of **2b** in methanol (red), acetonitrile (black), THF (green) and toluene (blue).

the absorption maxima observed in the near-UV regions (below 300 nm) are caused by $\pi \rightarrow \pi^*$ transitions involving the phenolate units. Intense, high energy bands are also observed in the region between 330 and 450 nm, which are assigned to charge transfer transitions from the out-of-plane pπ orbital (HOMO) of the phenolate oxygen to the half-filled $d_{x^2-y^2}/d_{z^2}$ orbital of high-spin Fe(III). The lowest energy bands (between 450 and 700 nm) are proposed to arise from charge-transfer transitions from the in-plane pπ orbital of the phenolate to the half-filled dπ^* orbital of Fe(III). A shift of these LMCT bands is observed on changing the solvent used. Representative electronic absorption spectra of **1b**, **2b** and **4b** are shown in Fig. 10, 11, and 12, respectively. In all complexes, the lowest energy LMCT bands exhibit noticeable solvent-dependent shifts according to the following trend: methanol < tetrahydrofuran < toluene < acetonitrile. In **1b**, the absorption spectrum in acetonitrile shows this band at lowest wavelength (489 nm) down from 562 nm in methanol. The absorption spectra in toluene and THF display this LMCT band at 498 and 538 nm, respectively. In complex **2b**, a similar trend in solvent effect is observed giving LMCT bands at 560, 541, 493, and 490 nm, respectively, whereas **4b** shows this band at

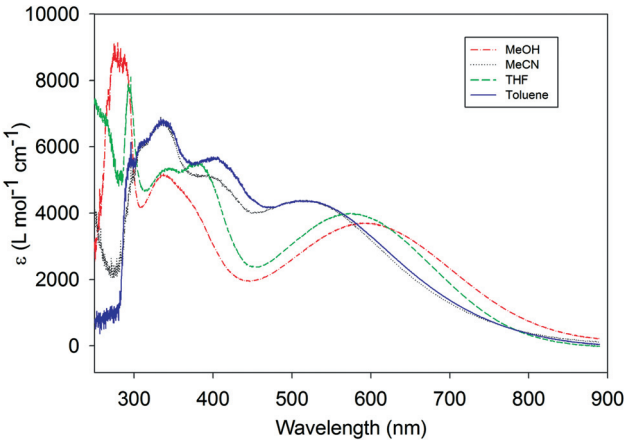

Fig. 12 Electronic absorption spectra of **4b** in methanol (red), acetonitrile (black), THF (green) and toluene (blue).

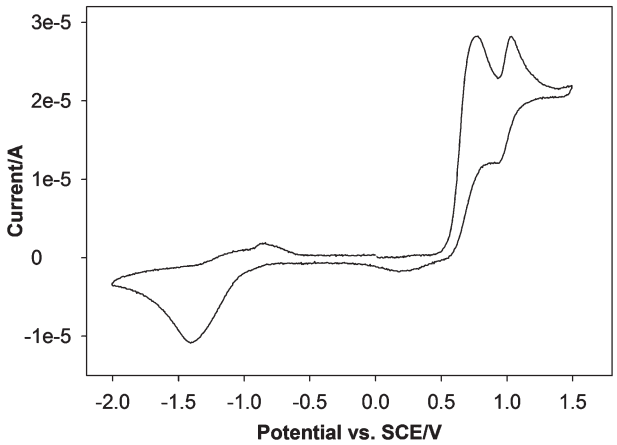

Fig. 13 Cyclic voltammagram of FeBr$[O_2NO]^{BuMeMeth}$, **4b**, in acetonitrile (0.1 M $[(n\text{-}Bu)_4N]PF_6$) at 20 °C and a scan rate of 100 mV s^{-1}.

592, 566, 517 and 515 nm in each of methanol, THF, toluene and acetonitrile. While variation in transition frequency due to solvatochromism can be expected upon changing the polarity of the solvent, the trends may also be influenced if the solvent affects the metal coordination sphere. The halide ligands are anticipated to be labile in solution,[44] hence coordinating solvents such as methanol, THF and acetonitrile would clearly interact with the iron(III) centers influencing the ligand fields and the electronic spectra. Therefore, whereas solvent polarities (as determined by dielectric constants) increase in the order of toluene, THF, methanol and acetonitrile, the ligand field strengths of these solvents affect the energies of the metal-centered orbitals. The high polarity of acetonitrile should result in a larger red-shift than THF or methanol, but this effect is likely influenced by a change in the ligand field resulting from coordination of acetonitrile ligands.

Electrochemistry

The redox behavior of these complexes is highly dependent on conditions, including solvent, electrode and electrolyte. Compounds **1a** and **4b** were first investigated using cyclic voltammetry (CV) in acetonitrile solutions containing $LiClO_4$, $NaBF_4$ and $NaPF_6$ as electrolyte and using glassy carbon, platinum and gold working electrodes (see ESI†). However, ligand substitution ensues as the highly labile halide is readily exchanged in solutions containing these electrolytes, thus causing complicated and unassignable CVs. More assignable CVs were obtained for complexes **1b** and **4b** in acetonitrile using 0.1 M $[(n\text{-}Bu)_4N]PF_6$ as electrolyte and a glassy carbon electrode, whereas in dichloromethane the CVs were again, unassignable. A complete cyclic voltammagram of **4b** in acetonitrile at a scan rate of 100 mV s^{-1} is shown in Fig. 13 and CVs of **1b** and **4b** in acetonitrile showing only the positive potentials at various scan rates are shown in Fig. 14 and 15. The CVs of the Fe(III) complexes are similar and display an irreversible (or very weakly quasi-reversible) reduction wave at $E^1_{p,red} = -1.40$ V (where $E_{p,red}$ and $E_{p,ox}$ are the peak potentials for reduction and oxidation, respectively) and two oxidations. At scan rates of 500 mV s^{-1}, in **1b** both of the oxidations approach reversible behavior and exhibit waves at

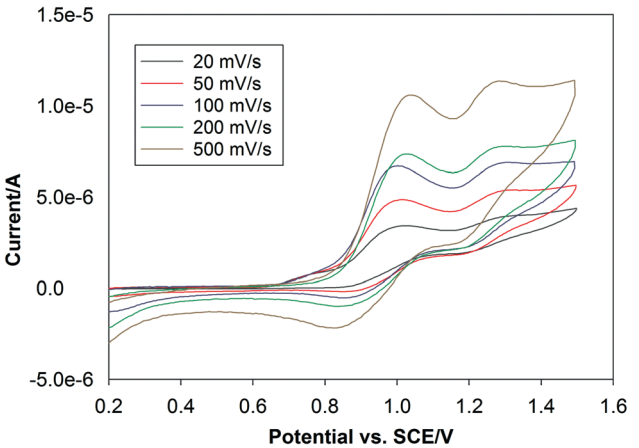

Fig. 14 Cyclic voltammagram (oxidation potentials) of FeBr$[O_2NO]^{BuBuFurf}$, **1b**, in acetonitrile (0.1 M $[(n\text{-}Bu)_4N]PF_6$) at 20 °C and scan rates as shown.

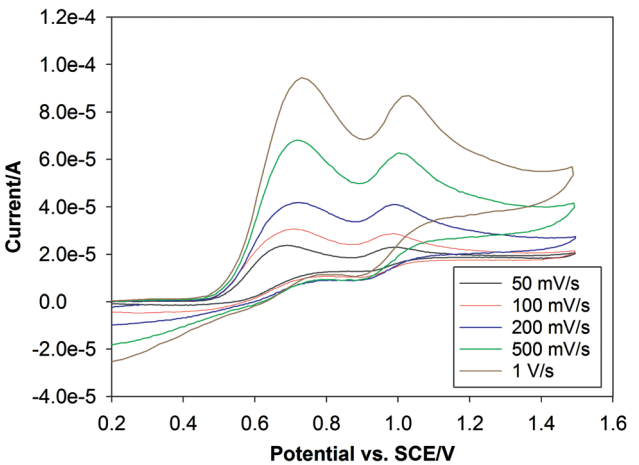

Fig. 15 Cyclic voltammagram (oxidation potentials) of FeBr$[O_2NO]^{BuMeMeth}$, **4b**, in acetonitrile (0.1 M $[(n\text{-}Bu)_4N]PF_6$) at 20 °C and scan rates as shown.

$E^2_{1/2}$ = +0.93 V ($E^2_{p,ox}$ = +1.03 V and $E^2_{p,red}$ = +0.83 V) and $E^3_{1/2}$ = +1.23 V ($E^3_{p,ox}$ = +1.27 V and $E^3_{p,red}$ = +1.19 V), whereas in **4b** the first oxidation shows very limited reversibility, $E^2_{p,ox}$ = +0.72 V, but the second is reversible, $E^3_{1/2}$ = +0.96 V ($E^3_{p,ox}$ = +1.00 V and $E^3_{p,red}$ = +0.92 V). While the ratios of the currents I_{red}/I_{ox} for $E^2_{p,ox}$ for **4b** at small velocities are below 1, they approach 1 with increasing scan rates. Thus, at high scan rates reduction becomes kinetically possible from double oxidized $\mathbf{4b}^{2+}$. Also, $E^2_{p,ox}$ and $E^3_{p,ox}$ in **4b** are shifted cathodically in comparison to **1b** by 0.32 and 0.27 V, respectively, at scan rates of 500 mV s^{-1}. This implies oxidized $\mathbf{4b}^{+}$ is stabilized in comparison to $\mathbf{1b}^{+}$. The overall electrochemical behavior of these Fe(III) complexes is similar to that observed in Cr(III) and Co(II) complexes of these or related ligands reported by us,[34,72] and others for a variety of metals.[39–41,63] Therefore, the relatively minor influence of the metal on the oxidation behavior of these complexes strongly suggests oxidation occurs at the ligand, resulting in the formation of Fe(III) phenoxyl and diphenoxyl radical species, $FeBr\mathbf{Ln}^{+}$ and $FeBr\mathbf{Ln}^{2+}$, respectively. The irreversible reductions at negative potentials are likely Fe(III)–Fe(II) couples in **1a**, **1b**, and **4b**.

Conclusions

A series of iron(III) complexes supported by amine–bis(phenolate) ligands has been prepared. All structurally characterized complexes reported are five-coordinate and exhibit mildly distorted trigonal bipyramidal geometries. Representative complexes **1b**, **2b**, and **4b**, and proligand $H_2\mathbf{L4}$ have been structurally characterized by single crystal X-ray diffraction. Additionally, all of the paramagnetic complexes have been analytically verified by elemental analysis and MALDI-TOF mass spectrometry. Magnetic moment measurements confirm high-spin d^5 electronic configurations. Mössbauer spectroscopy was performed on representative complexes, which also confirmed their oxidation and spin behavior. Electronic absorption spectra in the UV-visible range exhibit strong charge transfer bands, which are strongly solvent dependent and rapid exchange of the halide (chloride or bromide) ligand in solution with strongly coordination solvents is expected.

Experimental

General methods and materials

Unless otherwise stated, all manipulations were performed under an atmosphere of dry oxygen-free nitrogen by means of Schlenk techniques or using an MBraun Labmaster DP glove box. Anhydrous diethyl ether and toluene were purified using an MBraun Solvent Purification System. THF was stored over sieves and distilled from sodium benzophenone ketyl under nitrogen. Methanol and acetonitrile were dried over calcium hydride and distilled under nitrogen. Reagents were purchased either from Strem, Aldrich or Alfa Aesar and used without further purification. The proligands were prepared by the previously reported methods ($H_2\mathbf{L1}$,[13] $H_2\mathbf{L2}$[65] and $H_2\mathbf{L3}$[23,73]) but in aqueous medium. Anhydrous $FeCl_3$ (97%) from Aldrich was used for the synthesis of **1a–4a**. Anhydrous $FeBr_3$ (99%) was obtained from Strem Chemicals for the preparation of **1b–4b**.

NMR spectra were recorded in $CDCl_3$ on Bruker Avance-500 or AvanceIII-300 spectrometers and referenced internally to TMS. MALDI-TOF MS spectra were recorded on an Applied Biosystems Voyager DE-PRO equipped with a reflectron, delayed ion extraction and high performance nitrogen laser (337 nm). Samples were prepared at a concentration of 0.03 mg L^{-1} in methanol. Anthracene was used as the matrix, which was mixed at a concentration of 0.03 mg L^{-1}. UV-vis spectra were recorded on an Ocean Optics USB4000+ spectrophotometer. Elemental analyses were carried out by Canadian Microanalytical Service Ltd, Delta, BC, Canada. Magnetic susceptibility data were acquired in the solid state using a Quantum Designs MPMS5 SQUID magnetometer for variable temperature measurements, or a Johnson-Mathey magnetic susceptibility balance at room temperature, which was calibrated using $Hg[Co(NCS)_4]$. The data were corrected for the diamagnetism of all atoms. Magnetic moments in solution were obtained using Evans' NMR method.[78] Cyclic voltammetry measurements of **1b** and **4b** were performed in acetonitrile with 0.1 M $[(n\text{-}Bu)_4N]PF_6$ as electrolyte using a three-compartment electrochemical cell consisting of a platinum counter electrode, saturated calomel reference electrode (SCE) and a glassy-carbon working electrode on a Model HA 301 Hokuto Deuko Potentiostat/Galvanostat. The electrochemistry of **1a** and **4b** using other electrolytes and electrodes is described in the ESI†. ^{57}Fe Mössbauer spectra were recorded using a W.E.B. Research Mössbauer spectroscopy system connected to a Janis Research variable temperature SHI-850 cryostat and a closed cycle refrigerator. A ^{57}Co (in rhodium matrix) source with a strength of ~40 mCi was used. The detector was a Reuters-Stokes Kr/CO_2 proportional counter. The sample powders were loaded in a high-density polyethylene flat washer (**3a** and **2b**) or a folded piece of parafilm (**4b**), and wrapped in Kapton tape. The velocity was scanned between 4 and −4 mm s^{-1} using a constant acceleration triangle waveform, and calibrated against an Fe foil measured at 295 K in zero magnetic field. All isomer shifts (δ) are relative to Fe foil. Fitting of the data was performed using WMOSS software, which is available free of charge at http://wmoss.org/.

X-Ray crystallography

Crystal structures were solved on an AFC8-Saturn 70 single crystal X-ray diffractometer from Rigaku/MSC, equipped with an X-stream 2000 low temperature system. Suitable crystals of $H_2\mathbf{L4}$, **1b**, **2b** and **4b** were selected and mounted on a diffraction loop using Paratone-N oil and cooled to 153 K or lower. All measurements were made on a Rigaku Saturn CCD area detector with graphite monochromated Mo-Kα radiation. The data were processed[79] and corrected for Lorentz and polarization effects and absorption.[80] Neutral atom scattering factors for all non-hydrogen atoms were taken from the International Tables for X-ray Crystallography.[81] Structures were solved by direct methods[82] and expanded using Fourier techniques.[83] All non-hydrogen atoms were refined anisotropically. Hydrogen atoms were refined using the riding model. Anomalous dispersion effects were included in F_{calc};[84] the values for $\Delta f'$ and $\Delta f''$ were those of Creagh and McAuley.[85] The values for the mass attenuation coefficients are those of Creagh and Hubbell.[86] All

calculations were performed using the CrystalStructure[87,88] crystallographic software package except for refinement, which was performed using SHELXL-97.[89]

Synthesis of compounds

$H_2[O_2NO]^{BuMeMeth}$ (H_2L4)

2-Methoxyethylamine (4.63 g, 0.0616 mol) was added dropwise to a vigorously stirred mixture of 2-*tert*-butyl-4-methylphenol (20.236 g, 0.1232 mol) and 37% aqueous formaldehyde (9.17 mL, 0.1232 mol) in water (50 mL). The resulting mixture was heated to reflux for 12 h. Upon cooling, a large quantity of white solid formed. The solvents were decanted and the remaining solids were washed with cold methanol to give an analytically pure, white powder (26.95 g, 95% yield). Crystalline product was obtained by slow cooling of a hot diethyl ether solution. ^{1}H NMR (300.13 MHz, 295 K, δ): 8.40 (s, 2H, OH); 7.0 (d, $^4J_{HH}$ = 1.5 Hz, 2H, ArH); 6.72 (d, $^4J_{HH}$ = 1.5 Hz, 2H, ArH); 3.71 (s, 4H, $ArCH_2$); 3.52 (t, $^3J_{HH}$ = 5.09 Hz, 2H, CH_2O); 3.46 (s, 3H, OCH_3); 2.73 (t, $^3J_{HH}$ = 5.09 Hz, 2H, NCH_2); 2.24 (s, 6H, $ArCH_3$); 1.41 (s, 18H, $ArC(CH_3)_3$). ^{13}C{H} (75.47 MHz, 295 K, δ): 153.04 (Ar–*C*–OH); 136.83 (Ar–*C*H); 128.79 (Ar–*C*H); 127.36 (Ar–*C*H); 127.24 (Ar–*C*H); 122.44 (Ar–*C*–CH_2–N); 71.51 (Ar–CH_2); 58.86 (OCH_3); 51.37 (N–CH_2–CH_2–O); 57.62(N–CH_2–CH_2–O); 34.71 ($C(CH_3)_3$); 29.57 ($C(CH_3)_3$); 20.78 (Ar–CH_3). IR (cm^{-1}): 3350 (OH); 2955 (C–H); 1603 (C=C, phenyl ring). Anal. Calcd for $C_{27}H_{41}NO_3$: C, 75.84; H, 9.66; N, 3.28. Found C, 75.86; H, 9.69; N, 3.30.

FeClL1 (1a)

To a slurry of recrystallized $H_2[O_2NO]^{BuBuFurf}$, H_2**L1** (3.51 g, 6.52 mmol) in methanol was added a solution of anhydrous $FeCl_3$ (1.06 g, 6.52 mmol) in methanol resulting in an intense blue solution. To this solution was added triethylamine (1.32 g, 13.0 mmol) and the resulting mixture was stirred for 2 h. Solvent was removed under vacuum; the residue was extracted with acetone and filtered through Celite. Removal of solvent under vacuum yielded 3.64 g (89%) of analytically pure dark-blue product. Anal. Calcd for $C_{35}H_{53}ClFeNO_3$: C, 67.03; H, 8.52; N, 2.23. Found C, 67.32; H, 8.72; N, 2.32. MS (MALDI-TOF) *m*/*z* (%, ion): 626.31 (20, $[M]^+$), 591.34 (100, $[M - Cl]^+$). UV-vis (solvent) λ_{max}, nm (ε): (methanol) 616 (2670), 350 (2750). μ_{eff} (solution, 25 °C) 5.5 μ_B.

FeBrL1 (1b)

To a slurry of recrystallized $H_2[O_2NO]^{BuBuFurf}$, H_2**L1** (3.51 g, 6.52 mmol) in methanol was added a solution of anhydrous $FeBr_3$ (1.93 g, 6.52 mmol) in methanol resulting in an intense blue solution. To this solution was added triethylamine (1.32 g, 13.0 mmol) and the resulting mixture was stirred for 2 h. Solvent was removed under vacuum; the residue was extracted with acetone and filtered through Celite. Removal of solvent under vacuum yielded 3.79 g (90%) of analytically pure dark-purple product. Crystals suitable for X-ray diffraction were obtained by slow evaporation of a solution of **1b** in a 1 : 1 mixture of hexanes and acetone. Anal. Calcd for $C_{35}H_{53}BrFeNO_3$: C, 62.60; H, 7.95; N, 2.09. Found C, 62.52; H, 7.92; N, 2.19. MS (MALDI-TOF) *m*/*z* (%, ion): 670.26 (20, $[M]^+$), 591.34 (100, $[M - Br]^+$). UV-vis (solvent) λ_{max}, nm (ε): (methanol) 562 (2530), 335 (4000); (acetonitrile) 489 (3200), 400 (3800); (THF) 538 (2730), 381 (4210); (toluene) 498 (3180), 402 (4120). μ_{eff} (solution, 25 °C) 5.9 μ_B.

FeClL2 (2a)

The complex was synthesized according to the general method described for **1a**, and details have been reported elsewhere.[65]

Anal. Calcd for $C_{29}H_{41}ClFeNO_3$: C, 64.15; H, 7.61; N, 2.58. Found C, 64.35; H, 7.82; N, 2.88. MS (MALDI-TOF) *m*/*z* (%, ion): 542.21 (100, $[M]^+$), 507.24 (73, $[M - Cl]^+$). UV-vis (CH_3OH) λ_{max}, nm (ε): 616 (1670), 350 (1750). μ_{eff} (solid, 25 °C) 5.9 μ_B.

FeBrL2 (2b)

The complex was synthesized according to the general method described for **1b** using proligand H_2**L2**. Anal. Calcd for $C_{29}H_{41}BrFeNO_3$: C, 59.30; H, 7.04; N, 2.38. Found C, 59.52; H, 7.12; N, 2.39. MS (MALDI-TOF) *m*/*z* (%, ion): 586.16 (20, $[M]^+$), 507.24 (100, $[M - Br]^+$). UV-vis (solvent) λ_{max}, nm (ε): (methanol) 560 (2230), 374 (3560); (acetonitrile) 490 (2400), 400 (2850); (THF) 541 (1840), 339 (3050); (toluene) 493 (2350), 406 (3070). μ_{eff} (solid, 25 °C) 5.9 μ_B.

FeClL3 (3a)

The complex was synthesized according to the method described for **1a** using proligand H_2**L3**. Anal. Calcd for $C_{33}H_{51}ClFeNO_3$: C, 65.94; H, 8.55; N, 2.33. Found C, 65.92; H, 9.62; N, 2.29. MS (MALDI-TOF) *m*/*z* (%, ion): 600.29 (20, $[M]^+$), 565.32 (100, $[M - Cl]^+$). UV-vis (solvent) λ_{max}, nm (ε): (methanol) 560 (2230), 374 (3560); (acetonitrile) 490 (2400), 400 (2850); (THF) 541 (1840), 339 (3050); (toluene) 493 (2350), 406 (3070). μ_{eff} (solid, 25 °C) 5.5 μ_B.

FeBrL3 (3b)

The complex was synthesized according to the method described for **1b** using proligand H_2**L3**. Anal. Calcd for $C_{33}H_{51}BrFeNO_3$: C, 61.40; H, 7.96; N, 2.17. Found C, 61.52; H, 7.92; N, 2.19. MS (MALDI-TOF) *m*/*z* (%, ion): 600.29 (20, $[M]^+$), 565.32 (100, $[M - Br]^+$). UV-vis (solvent) λ_{max}, nm (ε): (methanol) 560 (2230), 374 (3560); (acetonitrile) 490 (2400), 400 (2850); (THF) 541 (1840), 339 (3050); (toluene) 493 (2350), 406 (3070). μ_{eff} (solution, 25 °C) 5.8 μ_B.

FeClL4 (4a)

The complex was synthesized according to the method described for **1a** using proligand H_2**L4**. Anal. Calcd for $C_{27}H_{39}ClFeNO_3$: C, 62.74; H, 7.60; N, 2.71. Found C, 62.82; H, 7.62; N, 2.79. MS (MALDI-TOF) *m*/*z* (%, ion): 516.20 (20, $[M]^+$), 481.23 (100, $[M - Cl]^+$). UV-vis (solvent) λ_{max}, nm (ε): (methanol) 592 (3680), 331 (5000); (acetonitrile) 515 (4200), 400 (5000); (THF) 566 (4000), 339 (5800); (toluene) 517 (4500), 406 (5900). μ_{eff} (solution, 25 °C) 5.7 μ_B.

FeBrL4 (4b)

The complex was synthesized according to the method described for **1b** using proligand H_2**L4**. Anal. Calcd for $C_{27}H_{39}BrFeNO_3$: C, 57.77; H, 7.00; N, 2.50. Found C, 57.92; H, 7.02; N, 2.55. MS (MALDI-TOF) *m/z* (%, ion): 560.15 (20, $[M]^+$), 481.23 (100, $[M - Br]^+$). UV-vis (solvent) λ_{max}, nm (ε): (methanol) 592 (3680), 331 (5000); (acetonitrile) 515 (4200), 400 (5000); (THF) 566 (4000), 339 (5800); (toluene) 517 (4500), 406 (5900). μ_{eff} (solid, 25 °C) 5.7 μ_B.

Acknowledgements

This research was supported by the Natural Sciences and Engineering Research Council (NSERC) of Canada (Discovery and Research Tools and Instruments Grants to C.M.K., D.B.L. and H.-B.K., Postgraduate Scholarship to R.K.D, Undergraduate Student Research Award to P.K.) the Canada Foundation for Innovation (Leaders Opportunity Fund to C.M.K.) and the Provincial Government of Newfoundland and Labrador (RDC/IRIF grants to C.M.K). K.H. thanks Memorial University of Newfoundland School of Graduate Studies for funding. P.K. thanks the Inorganic Chemistry Exchange (ICE) program of the Chemical Institute of Canada (Inorganic Division) for facilitating aspects of this research.

References

1 A. Yeori, I. Goldberg and M. Kol, *Macromolecules*, 2007, **40**, 8521–8523.
2 A. Yeori, I. Goldberg, M. Shuster and M. Kol, *J. Am. Chem. Soc.*, 2006, **128**, 13062–13063.
3 S. Gendler, S. Segal, I. Goldberg, Z. Goldschmidt and M. Kol, *Inorg. Chem.*, 2006, **45**, 4783–4790.
4 S. Segal, I. Goldberg and M. Kol, *Organometallics*, 2005, **24**, 200–202.
5 S. Groysman, I. Goldberg, M. Kol, E. Genizi and Z. Goldschmidt, *Organometallics*, 2004, **23**, 1880–1890.
6 C. Lorber, F. Wolff, R. Choukroun and L. Vendier, *Eur. J. Inorg. Chem.*, 2005, 2850–2859.
7 A. J. Chmura, M. G. Davidson, M. D. Jones, M. D. Lunn, M. F. Mahon, A. F. Johnson, P. Khunkamchoo, S. L. Roberts and S. S. F. Wong, *Macromolecules*, 2006, **39**, 7250–7257.
8 E. Y. Tshuva, I. Goldberg and M. Kol, *J. Am. Chem. Soc.*, 2000, **122**, 10706–10707.
9 Y. Sarazin, R. H. Howard, D. L. Hughes, S. M. Humphrey and M. Bochmann, *Dalton Trans.*, 2006, 340–350.
10 C. L. Boyd, T. Toupance, B. R. Tyrrell, B. D. Ward, C. R. Wilson, A. R. Cowley and P. Mountford, *Organometallics*, 2005, **24**, 309–330.
11 S. Gendler, S. Groysman, Z. Goldschmidt, M. Shuster and M. Kol, *J. Polym. Sci., Part A: Polym. Chem.*, 2006, **44**, 1136–1146.
12 S. Groysman, I. Goldberg, M. Kol, E. Genizi and Z. Goldschmidt, *Organometallics*, 2003, **22**, 3013–3015.
13 S. Groysman, I. Goldberg, M. Kol, E. Genizi and Z. Goldschmidt, *Inorg. Chim. Acta*, 2003, **345**, 137–144.
14 S. Groysman, E. Y. Tshuva, I. Goldberg, M. Kol, Z. Goldschmidt and M. Shuster, *Organometallics*, 2004, **23**, 5291–5299.
15 M. Kol, E. Y. Tshuva, S. Groysman, S. Segal, I. Goldberg and Z. Goldschmidt, *PMSE Prepr.*, 2002, **86**, 304–305.
16 J. Lee, Y. Hong, J. H. Kim, S. H. Kim, Y. Do, Y. K. Shin and Y. Kim, *J. Organomet. Chem.*, 2008, **693**, 3715–3721.
17 L. Michalczyk, S. de Gala and J. W. Bruno, *Organometallics*, 2001, **20**, 5547–5556.
18 K. Mikami, Y. Matsumoto and T. Shiono, *Sci. Synth.*, 2003, **2**, 457–679.
19 E. Y. Tshuva, I. Goldberg, M. Kol and Z. Goldschmidt, *Inorg. Chem. Commun.*, 2000, **3**, 611–614.
20 E. Y. Tshuva, I. Goldberg, M. Kol and Z. Goldschmidt, *Chem. Commun.*, 2001, 2120–2121.
21 S. E. Reybuck, A. L. Lincoln, S. Ma and R. M. Waymouth, *Macromolecules*, 2005, **38**, 2552–2558.
22 S. Groysman, E. Y. Tshuva, D. Reshef, S. Gendler, I. Goldberg, M. Kol, Z. Goldschmidt, M. Shuster and G. Lidor, *Isr. J. Chem.*, 2003, **42**, 373–381.
23 E. Y. Tshuva, S. Groysman, I. Goldberg, M. Kol and Z. Goldschmidt, *Organometallics*, 2002, **21**, 662–670.
24 E. Y. Tshuva, I. Goldberg, M. Kol and Z. Goldschmidt, *Organometallics*, 2001, **20**, 3017–3028.
25 T. Toupance, S. R. Dubberley, N. H. Rees, B. R. Tyrrell and P. Mountford, *Organometallics*, 2002, **21**, 1367–1382.
26 S. Groysman, I. Goldberg, M. Kol, E. Genizi and Z. Goldschmidt, *Adv. Synth. Catal.*, 2005, **347**, 409–415.
27 S. Groysman, I. Goldberg, M. Kol and Z. Goldschmidt, *Organometallics*, 2003, **22**, 3793–3795.
28 F. M. Kerton, A. C. Whitwood and C. E. Willans, *Dalton Trans.*, 2004, 2237–2244.
29 H. E. Dyer, S. Huijser, A. D. Schwarz, C. Wang, R. Duchateau and P. Mountford, *Dalton Trans.*, 2008, 32–35.
30 F. Bonnet, A. R. Cowley and P. Mountford, *Inorg. Chem.*, 2005, **44**, 9046–9055.
31 A. Amgoune, C. M. Thomas and J. F. Carpentier, *Pure Appl. Chem.*, 2007, **79**, 2013–2030.
32 A. Amgoune, C. M. Thomas, T. Roisnel and J. F. Carpentier, *Chem.–Eur. J.*, 2006, **12**, 169–179.
33 Y. Yao, M. Ma, X. Xu, Y. Zhang, Q. Shen and W. T. Wong, *Organometallics*, 2005, **24**, 4014–4020.
34 U. K. Das, J. Bobak, C. Fowler, S. E. Hann, C. F. Petten, L. N. Dawe, A. Decken, F. M. Kerton and C. M. Kozak, *Dalton Trans.*, 2010, 5462–5477.
35 T. Nagataki and S. Itoh, *Chem. Lett.*, 2007, 748–749.
36 L. Rodríguez, E. Labisbal, A. Sousa-Pedrares, J. A. García-Vázquez, J. Romero, M. L. Durán, J. A. Real and A. Sousa, *Inorg. Chem.*, 2006, **45**, 7903–7914.
37 A. Philibert, F. Thomas, C. Philouze, S. Hamman, E. Saint-Aman and J.-L. Pierre, *Chem.–Eur. J.*, 2003, **9**, 3803–3812.
38 O. Rotthaus, F. Thomas, O. Jarjayes, C. Philouze, E. Saint-Aman and J.-L. Pierre, *Chem.–Eur. J.*, 2006, **12**, 6953–6962.
39 J. B. H. Strautmann, S. De Beer George, E. Bothe, E. Bill, T. Weyhermuller, A. Stammler, H. Bogge and T. Glaser, *Inorg. Chem.*, 2008, **47**, 6804–6824.
40 T. Weyhermuller, T. K. Paine, E. Bothe, E. Bill and P. Chaudhuri, *Inorg. Chim. Acta*, 2002, **337**, 344–356.
41 E. Safaei, T. Weyhermuller, E. Bothe, K. Wieghardt and P. Chaudhuri, *Eur.J. Inorg. Chem.*, 2007, 2334–2344.
42 R. Viswanathan, M. Palaniandavar, T. Balasubramanian and T. P. Muthiah, *Inorg. Chem.*, 1998, **37**, 2943–2951.
43 M. Velusamy, R. Mayilmurugan and M. Palaniandavar, *Inorg. Chem.*, 2004, **43**, 6284–6293.
44 M. Velusamy, M. Palaniandavar, R. S. Gopalan and G. U. Kulkarni, *Inorg. Chem.*, 2003, **42**, 8283–8293.
45 M. Merkel, F. K. Muller and B. Krebs, *Inorg. Chim. Acta*, 2002, **337**, 308–316.
46 L. Dyers, S. Y. Que, D. VanDerveer and X. R. Bu, *Inorg. Chim. Acta*, 2006, **359**, 197–203.
47 T. Kurahashi, Y. Kobayashi, S. Nagatomo, T. Tosha, T. Kitagawa and H. Fujii, *Inorg. Chem.*, 2005, **44**, 8156–8166.
48 T. Kurahashi, K. Oda, M. Sugimoto, T. Ogura and H. Fujii, *Inorg. Chem.*, 2006, **45**, 7709–7721.
49 D. J. Darensbourg, C. G. Ortiz and D. R. Billodeaux, *Inorg. Chim. Acta*, 2004, **357**, 2143–2149.
50 G. Ilyashenko, M. Motevalli and M. Watkinson, *Tetrahedron: Asymmetry*, 2006, **17**, 1625–1628.
51 R. Mayilmurugan, H. Stoeckli-Evans, E. Suresh and M. Palaniandavar, *Dalton Trans.*, 2009, 5101–5114.
52 J. B. H. Strautmann, C.-G. Freiherr von Richthofen, S. DeBeer George, E. Bothe, E. Bill and T. Glaser, *Chem. Commun.*, 2009, 2637–2639.
53 J. B. H. Strautmann, C.-G. Freiherr von Richthofen, G. Heinze-Brückner, S. DeBeer, E. Bothe, E. Bill, T. Weyhermüller, A. Stammler, H. Bögge and T. Glaser, *Inorg. Chem.*, 2011, **50**, 155–171.
54 C. J. Whiteoak, R. T. Martin de Rosales, A. J. P. White and G. J. P. Britovsek, *Inorg. Chem.*, 2010, **49**, 11106–11117.
55 H. Egami and T. Katsuki, *J. Am. Chem. Soc.*, 2007, **129**, 8940–8941.
56 H. Egami and T. Katsuki, *Synlett*, 2008, 1543–1546.
57 K. Hasan, C. Fowler, P. Kwong, A. K. Crane, J. L. Collins and C. M. Kozak, *Dalton Trans.*, 2008, 2991–2998.
58 T. Glaser, R. H. Pawelke and M. Heidemeier, *Z. Anorg. Allg. Chem.*, 2003, **629**, 2274–2281.

59 P. Mialane, E. Anxolabéhère-Mallart, G. Blondin, A. Nivorojkine, J. Guilhem, L. Tchertanova, M. Cesario, N. Ravi, E. Bominaar, J. J. Girerd and E. Münck, *Inorg. Chim. Acta*, 1997, **263**, 367–378.
60 R. Mayilmurugan, K. Visvaganesan, E. Suresh and M. Palaniandavar, *Inorg. Chem.*, 2009, **48**, 8771–8783.
61 A. M. Reckling, D. Martin, L. N. Dawe, A. Decken and C. M. Kozak, *J. Organomet. Chem.*, 2011, **696**, 787–794.
62 T. Weyhermueller, R. Wagner and P. Chaudhuri, *Eur. J. Inorg. Chem.*, 2011, 2547–2557.
63 R. Van Gorkum, J. Berding, A. M. Mills, H. Kooijman, D. M. Tooke, A. L. Spek, I. Mutikainen, U. Turpeinen, J. Reedijk and E. Bouwman, *Eur. J. Inorg. Chem.*, 2008, 1487–1496.
64 R. Van Gorkum, J. Berding, D. M. Tooke, A. L. Spek, J. Reedijk and E. Bouwman, *J. Catal.*, 2007, **252**, 110–118.
65 R. R. Chowdhury, A. K. Crane, C. Fowler, P. Kwong and C. M. Kozak, *Chem. Commun.*, 2008, 94–96.
66 E. Safaei, H. Sheykhi, A. Wojtczak, Z. Jaglicic and A. Kozakiewicz, *Polyhedron*, 2011, **30**, 1219–1224.
67 L. H. Tong, Y.-L. Wong, S. I. Pascu and J. R. Dilworth, *Dalton Trans.*, 2008, 4784–4791.
68 J. Hwang, K. Govindaswamy and S. A. Koch, *Chem. Commun.*, 1998, 1667–1668.
69 X. Qian, L. N. Dawe and C. M. Kozak, *Dalton Trans.*, 2011, 933–943.
70 R. Mayilmurugan, M. Sankaralingam, E. Suresh and M. Palaniandavar, *Dalton Trans.*, 2010, 9611–9625.
71 S. Mukherjee, T. Weyhermuller, E. Bill, K. Wieghardt and P. Chaudhuri, *Inorg. Chem.*, 2005, **44**, 7099–7108.
72 R. K. Dean, S. L. Granville, L. N. Dawe, A. Decken, K. M. Hattenhauer and C. M. Kozak, *Dalton Trans.*, 2010, 548–559.
73 F. M. Kerton, S. Holloway, A. Power, R. G. Soper, K. Sheridan, J. M. Lynam, A. C. Whitwood and C. E. Willans, *Can. J. Chem.*, 2008, **86**, 435–443.
74 K. L. Collins, L. J. Corbett, S. M. Butt, G. Madhurambal and F. M. Kerton, *Green Chem. Lett. Rev.*, 2008, **1**, 31.
75 In the previously reported structure of **2a**, the tetrahydrofurfuryl oxygen atom was labeled O(1) with phenolate oxygens labeled O(2) and O(3). For the purpose of consistency with the structures reported herein, O(1) and O(2) refer to the phenolate oxygens and O(3) refers to the neutral oxygen-donor on the pendant ether group.
76 H. L. Shyu, H. H. Wei, G. H. Lee and Y. Wang, *J. Chem. Soc., Dalton Trans.*, 2000, 915–918.
77 A. W. Addison, T. N. Rao, J. Reedijk, J. van Rijn and G. C. Verschoor, *J. Chem. Soc., Dalton Trans.*, 1984, 1349.
78 E. M. Schubert, *J. Chem. Educ.*, 1992, **69**, 62–62.
79 J. W. Pflugrath, *Acta Crystallogr., Sect. D: Biol. Crystallogr.*, 1999, **55**, 1718–1725.
80 A. C. Larson, *Crystallographic Computing*, Munksgaard, Copenhagen, 1970, pp. 291–294.
81 D. T. Cromer and J. T. Waber, *International Tables for X-ray Crystallography*, The Kynoch Press, Birmingham, England, 1974, vol. IV.
82 A. Altomare, G. Cascarano, C. Giacovazzo, A. Guagliardi, M. Burla, G. Polidori and M. Camalli, *J. Appl. Crystallogr.*, 1994, **27**, 435.
83 P. T. Beurskens, G. Admiraal, G. Beurskens, W. P. Bosman, R. de Gelder, R. Israel and J. M. M. Smits, *DIRDIF99*, University of Nijmegen, Netherlands, 1999.
84 J. A. Ibers and W. C. Hamilton, *Acta Crystallogr.*, 1964, **17**, 781.
85 D. C. Creagh and W. J. McAuley, *International Tables for Crystallography*, Kluwer Academic Publishers, Boston, 1992, vol. C, Table 4.2.6.8, pp. 219–222.
86 D. C. Creagh and J. H. Hubbell, *International Tables for Crystallography*, Kluwer Academic Publishers, Boston, 1992, vol. C, Table 4.2.4.3, pp. 200–206.
87 CrystalStructure 3.7.0: Crystal Structure Analysis Package, Rigaku and Rigaku/MSC, The Woodlands TX, 2000–2005.
88 D. J. Watkin, C. K. Prout, J. R. Carruthers and P. W. Betteridge, *CRYSTALS Issue 10*, Chemical Crystallography Laboratory, Oxford, UK, 1996.
89 G. M. Sheldrick, *Acta Crystallogr., Sect. A*, 2008, **64**, 112–122.

